

## Thermal-neutron scintillator: $\text{Ce}^{3+}$ activated $\text{Rb}_2\text{LiYBr}_6$

M. D. Birowosuto,<sup>a)</sup> P. Dorenbos,<sup>b)</sup> J. T. M. de Haas, and C. W. E. van Eijk  
*Radiation Detection and Matter, Faculty of Applied Sciences, Delft University of Technology, Mekelweg 15,  
 2629 JB, Delft, The Netherlands*

K. W. Krämer and H. U. Güdel  
*Department of Chemistry and Biochemistry, University of Bern, Freiestrasse 3, 3000 Bern 9, Switzerland*

(Received 7 November 2006; accepted 23 January 2007; published online 30 March 2007)

Scintillation and luminescence characteristics of  $\text{Rb}_2\text{LiYBr}_6$  doped with 0.1%, 0.5%, 1%, and 5%  $\text{Ce}^{3+}$  are presented. Under optical and x-ray excitation,  $\text{Ce}^{3+}$  doublet emission is observed at 385 and 420 nm.  $\text{Rb}_2\text{LiYBr}_6:0.5\% \text{Ce}^{3+}$  shows very high thermal neutron scintillation light output of 83 000 photons/neutron. An excellent neutron peak resolution of 3.6% (full width at half maximum over peak position) is observed for the 4.8 MeV neutron-reaction products energy response in  $\text{Rb}_2\text{LiYBr}_6:0.1\% \text{Ce}^{3+}$ . This peak shows up at 3.6 MeV  $\gamma$ -equivalent energy and therefore it gives an  $\alpha/\beta$  ratio of 0.74. The combination of a large fraction of neutron absorption in natural  ${}^6\text{Li}$  (62%), a sharp neutron response peak, high light yield, and large  $\alpha/\beta$  ratio makes  $\text{Rb}_2\text{LiYBr}_6:\text{Ce}^{3+}$  an efficient scintillator for thermal neutron detection. © 2007 American Institute of Physics.  
 [DOI: 10.1063/1.2713948]

Thermal neutron scattering is a powerful technique to study the structure and dynamics of materials.<sup>1</sup> For these studies, bright neutron sources are available; more intense sources are under construction. In April 2006, the accelerator of the Spallation Neutron Source (SNS), Oak Ridge, TN, was commissioned and the Japanese Neutron Spallation Source (JNNS), Tokai, Japan, will become operational in 2007.<sup>2,3</sup> For optimal use of the bright and pulsed sources, the development of advanced neutron detectors is very important. Furthermore, detection of radioactive and fissile materials by neutron detection is becoming increasingly important for inspection and security systems. Also for these applications, detector development is of interest.

There have been growing efforts in research and development of inorganic scintillators as neutron detectors based on the neutron capture reaction. Lithium-containing scintillators are among them.<sup>4</sup> They contain  ${}^6\text{Li}$  isotopes that capture thermal neutrons and convert them into ionizing particles according to the reaction



The two charged particles produced in the reaction have a total kinetic energy of 4.8 MeV and scintillation light is produced along their ionization tracks. The large kinetic energy offers an advantage whenever discrimination of neutrons against  $\gamma$ -background is a premium.<sup>4</sup>

Here, we report the scintillation and luminescence characteristics of  $\text{Rb}_2\text{LiYBr}_6$  doped with 0.1%, 0.5%, 1%, and 5%  $\text{Ce}^{3+}$ . This compound belongs to the elpasolite crystal structure family.<sup>5</sup> Scintillation properties under neutron excitation of various elpasolites were previously reported and they show high light yield and good neutron peak resolution.<sup>6–8</sup> In this work, we found that  $\text{Rb}_2\text{LiYBr}_6:\text{Ce}^{3+}$  shows the highest light yield (83 000 photons/neutron) and

the best neutron peak resolution (3.6%) among all studied elpasolites. The influence of  $\text{Ce}^{3+}$  concentration on the scintillation properties is also discussed.

Single crystals of  $\text{Rb}_2\text{LiYBr}_6:\text{Ce}^{3+}$  with calculated density of 3.82 g/cm<sup>3</sup> were grown by the vertical Bridgmann technique. They contain 7.5% natural abundance of  ${}^6\text{Li}$  isotopes. Approximately 62% of a fraction of incident thermal neutrons are captured by  ${}^6\text{Li}$  in  $\text{Rb}_2\text{LiYBr}_6$ . This fraction can be increased to 95% using 95% enrichment of  ${}^6\text{Li}$ . The crystals are hygroscopic, and experiments were performed on samples with sizes of 12–27 mm<sup>3</sup> sealed in quartz ampoules. A description of the experimental setups of radioluminescence, scintillation decay, and time-resolved emission and excitation measurements can be found in Birowosuto *et al.*<sup>9</sup> Details on the  $\gamma$ -ray and the thermal neutron scintillation pulse height measurement techniques can be found in Besiere *et al.*<sup>6</sup>

Figure 1 shows the radioluminescence spectra of 0.1%, 0.5%, 1%, and 5%  $\text{Ce}^{3+}$  doped  $\text{Rb}_2\text{LiYBr}_6$  at room temperature (RT). All spectra show a doublet emission band at 385 and 420 nm. This emission is caused by transitions from the lowest  $5d$  excited state of  $\text{Ce}^{3+}$  to the two spin orbit split  ${}^2F_{5/2}$  and  ${}^2F_{7/2}$  ground state levels. At low  $\text{Ce}^{3+}$  concentration, a contribution at 340 nm due to self-trapped emission (STE) is observed. When the  $\text{Ce}^{3+}$  concentration increases, this STE contribution disappears and the peak at 385 nm is shifted toward longer wavelength. This is due to the self-absorption of  $\text{Ce}^{3+}$  emission since the Stokes shift in bromoelpasolites is usually small (0.11–0.14 eV).<sup>9</sup>

Time-resolved emission and excitation spectra and optically excited decay curves of  $\text{Rb}_2\text{LiYBr}_6:0.5\% \text{Ce}^{3+}$  at 10 K are shown in Fig. 2. The excitation spectrum of the slow luminescence shows an excitation band peaking at 198 nm whereas that of the fast luminescence shows an excitation band above 310 nm; see Fig. 2(i). The band at 198 nm is assigned to excitation of the host lattice whereas that above 310 nm is attributed to the excitation of the lowest  $5d$

<sup>a)</sup>Electronic mail: m.d.birowosuto@tnw.tudelft.nl

<sup>b)</sup>Electronic mail: p.dorenbos@tnw.tudelft.nl

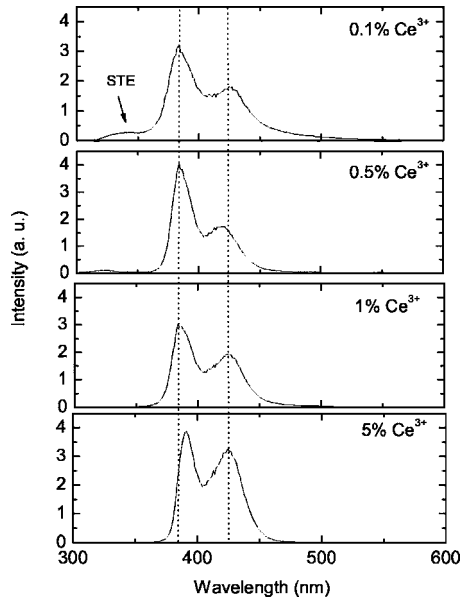


FIG. 1. Radioluminescence spectra at RT of  $\text{Rb}_2\text{LiYBr}_6$  doped with 0.1%, 0.5%, 1%, and 5%  $\text{Ce}^{3+}$ .

band of  $\text{Ce}^{3+}$ . Similar bands were previously observed in other  $\text{Ce}^{3+}$  doped bromoelpasolites like  $\text{Cs}_2\text{NaREBr}_6:\text{Ce}^{3+}$  ( $\text{RE}=\text{La}, \text{Y}, \text{Lu}$ ).<sup>9</sup> The band gap energy of  $\text{Rb}_2\text{LiYBr}_6$  ( $E_{\text{VC}}$ ) is estimated to be 8% higher than the energy of the 198 nm exciton creation peak. This band gap of 6.8 eV corresponds well with that of other bromoelpasolites.<sup>9</sup> When excited at 198 nm, the emission spectrum shows a doublet  $\text{Ce}^{3+}$  emission band and a slow band peaking at 500 nm; see Fig. 2(i). We attribute the broad slow band to STE emission.

The decay curve excited at the 333 nm  $5d$  band of  $\text{Ce}^{3+}$  is fitted with a single exponential decay of 24 ns; see inset (a) in Fig. 2. This decay time is the same as for  $\text{Ce}^{3+}$  in other bromoelpasolites.<sup>9</sup> When excited via the host lattice at 215 nm, two exponential decay components of 42 ns (53%) and 250 ns (47%) appear; see inset (b) in Fig. 2. These decay components are longer than the 24 ns lifetime of the  $5d$

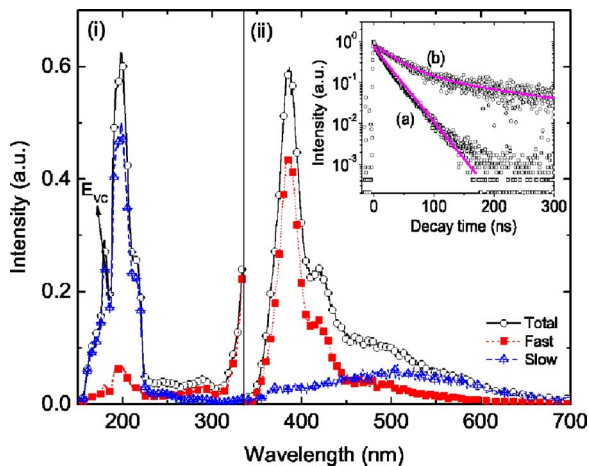


FIG. 2. (Color online) (i) Time-resolved excitation spectrum monitoring 387 nm and (ii) emission spectrum excited at 198 nm recorded at 10 K of  $\text{Rb}_2\text{LiYBr}_6:0.5\% \text{Ce}^{3+}$ . The inset shows decay curves at 10 K of  $\text{Rb}_2\text{LiYBr}_6:0.5\% \text{Ce}^{3+}$  (a) excited at 333 nm and monitoring at 386 nm and (b) excited at 215 nm and monitoring at 440 nm. The lines through the decay curves are mono- and biexponential fits.

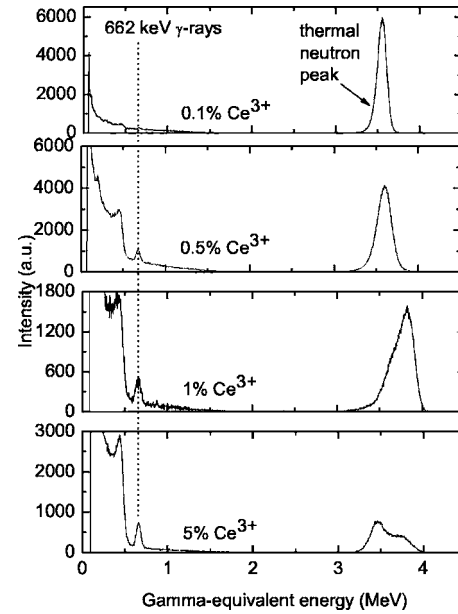


FIG. 3. The scintillation pulse height spectra of  $\text{Rb}_2\text{LiYBr}_6$  doped with 0.1%, 0.5%, 1%, and 5%  $\text{Ce}^{3+}$  at RT irradiated with  $\gamma$ -rays from a  $^{137}\text{Cs}$  source and thermal neutrons from a reactor beam line.

excited state of  $\text{Ce}^{3+}$ . Apparently, the electron-hole pairs are first trapped by the lattice and then transferred to  $\text{Ce}^{3+}$ . In addition, STE contributes to the decay curve since a remnant of STE emission is present at 440 nm.

Figure 3 shows  $\gamma$ -ray and thermal-neutron excited scintillation pulse height spectra of  $\text{Rb}_2\text{LiYBr}_6:\text{Ce}^{3+}$ . The 662 keV peak was used to calibrate the spectra in  $\gamma$ -equivalent energy. It is assumed that nonlinearity effects are negligible at higher energy. For all spectra, a distinct neutron peak shows up at energies around 3.5 MeV  $\gamma$ -equivalent energy.

The scintillation light yield (LY) obtained with  $\gamma$ -rays, expressed as the number of photons emitted per MeV absorbed  $\gamma$ -ray energy (photons/MeV), the light yield per thermal neutron (photon/neutron), the peak resolution  $R_{662}$  of the 662 keV  $\gamma$ -peak, the peak resolution  $R_n$  of the thermal neutron peak, and the ratio  $\alpha/\beta$  between  $\gamma$ -equivalent energy of the neutron peak and the total kinetic energy of 4.8 MeV are compiled in Table I. Light yield and energy resolution obtained with  $\gamma$ -rays were derived from  $\gamma$ -ray excited scintillation pulse height spectra (not shown), whereas those of thermal neutron were derived from Fig. 3. The highest thermal neutron scintillation light yield of 83 000 photons/neutron is

TABLE I. Light yields and energy resolutions of  $\text{Rb}_2\text{LiYBr}_6:\text{Ce}^{3+}$  under  $\gamma$ -ray and thermal neutron irradiation. They were derived from pulse-height spectra with a 10  $\mu\text{s}$  shaping time.

	$^{137}\text{Cs}$ $\gamma$ -rays		Thermal neutron		
	LY (photons/MeV)	$R_{662}$ (%)	LY (photons/neutron)	$R_n$ (%)	$\alpha/\beta$
0.1% $\text{Ce}^{3+}$	16 500	5.3	59 000	3.6	0.74
0.5% $\text{Ce}^{3+}$	23 000	4.7	83 000	5.4	0.75
1% $\text{Ce}^{3+}$	~13 000	-	49 000	8.5	~0.79
5% $\text{Ce}^{3+}$	~13 000	-	51 000	4.2	~0.82
	~11 000	-	39 000	5.8	~0.74
	~11 000	-	42 000	7.8	~0.80

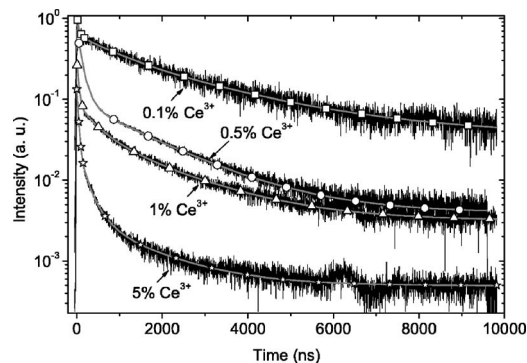


FIG. 4. The scintillation decay curves of  $\text{Rb}_2\text{LiYBr}_6$  doped with 0.1%, 0.5%, 1%, and 5%  $\text{Ce}^{3+}$  at RT under 662 keV  $\gamma$ -ray excitation. The lines through the curves are the summed exponential fits.

recorded for  $\text{Rb}_2\text{LiYBr}_6:0.5\% \text{Ce}^{3+}$ , whereas the best neutron peak resolution of 3.6% is recorded for  $\text{Rb}_2\text{LiYBr}_6:0.1\% \text{Ce}^{3+}$ . The neutron peak shape appears to deteriorate when the  $\text{Ce}^{3+}$  concentration increases. The neutron peaks of  $\text{Rb}_2\text{LiYBr}_6:1\%$  and  $5\% \text{Ce}^{3+}$  are even composed of two subpeaks. Presumably one part of the crystal produces more photons than another part. For the 1% and 5%  $\text{Ce}^{3+}$  crystals, yields and resolutions of both subpeaks are listed in Table I. For the 662 keV complex lines, we do not give energy-resolution values in Table I as unfolding results in large errors. To determine more accurately how the energy-peak resolution depends on  $\text{Ce}^{3+}$  concentration, better crystals will have to be grown.

The light yield decreases by a factor of 2 when the concentration increases from 0.5 to 5%. The  $\alpha/\beta$  ratio varies between 0.74 and 0.80. This ratio is larger than those of 0.31 of  ${}^6\text{Li}$  glass and 0.45 of  ${}^6\text{LiF-ZnS:Ag}$ .<sup>8</sup>

Figure 4 shows the  $\gamma$ -excited scintillation decay curves of  $\text{Rb}_2\text{LiYBr}_6:\text{Ce}^{3+}$  at RT recorded using the single photon counting technique.<sup>10</sup> The neutron-excited scintillation decay curves were also recorded. They are identical to those excited by  $\gamma$ -rays. The decay curves were fitted with three exponentials and the decay components with their relative contributions to the total light yield are presented in Table II.

The decay time of the fast component (42 ns) is slower than the decay time of the  $\text{Ce}^{3+}$  emission when excited directly in the  $5d$  state (24 ns at 10 K); see the inset in Fig. 2. This means that direct charge carrier capture in  $\text{Ce}^{3+}$  is not a dominant process in  $\text{Rb}_2\text{LiYBr}_6$ . Instead, we recently proposed energy transfer by binary electron-hole diffusion as the dominant scintillation mechanism.<sup>9</sup> The majority of the electrons and holes form an impurity perturbed STE, which is relatively stable in undoped and  $\text{Ce}^{3+}$  doped  $\text{Rb}_2\text{LiYBr}_6$ . Assuming that in both cases free electrons move faster than free holes, fast  $\text{Ce}^{3+}$  luminescence is observed if the diffusion rate of the holes is of the order of magnitude of the time required to create a STE. Since this process is dependent on  $\text{Ce}^{3+}$  concentration, it is expected that increasing the  $\text{Ce}^{3+}$  concentration will lead to an increase in the contribution of the fast component to the light yield. From Table II, the contribution of the fast component to the total light yield increases from 1 to 35% with increasing  $\text{Ce}^{3+}$  concentration.

TABLE II. Characteristic components of the scintillation decay curves of  $\text{Rb}_2\text{LiYBr}_6$  doped with 0.1%, 0.5%, 1%, and 5%  $\text{Ce}^{3+}$ .

$\text{Rb}_2\text{LiYBr}_6$	Decay components		
	(relative contribution to light yield within 10 $\mu\text{s}$ )		
	Fast (ns)	Intermediate (ns)	Slow (ns)
0.1% $\text{Ce}^{3+}$	42 (1%)	870 (17%)	2700 (82%)
0.5% $\text{Ce}^{3+}$	42 (3%)	140 (23%)	1600 (74%)
1% $\text{Ce}^{3+}$	42 (11%)	450 (22%)	1800 (67%)
5% $\text{Ce}^{3+}$	42 (35%)	250 (32%)	1400 (33%)

In conclusion, the properties presented in this work for  $\text{Rb}_2\text{LiYBr}_6:\text{Ce}^{3+}$  demonstrate that this material is a good thermal neutron scintillator. The light yield of 83 000 photons/neutron is higher than the 51 000 photons/neutron of the well-known  ${}^6\text{LiI:Eu}^{2+}$  thermal neutron scintillator.<sup>8,11</sup> The neutron peak resolution of 3.6% is the best ever reported for a thermal neutron scintillator. This energy resolution is better than the 3.9% resolution of  ${}^6\text{LiI:Eu}^{2+}$  and the 4.6% resolution of  $\text{Cs}_2\text{LiYBr}_6:\text{Ce}^{3+}$ .<sup>8,11</sup> Together with the large  $\alpha/\beta$  ratio in Table I,  $\text{Rb}_2\text{LiYBr}_6:\text{Ce}^{3+}$  offers the possibility of excellent neutron/ $\gamma$  discrimination. Additionally, the scintillation decay curve of  $\text{Rb}_2\text{LiYBr}_6:\text{Ce}^{3+}$  shows relatively fast components of 42 and 140 ns. Together with the high light yield, this makes the new material better for timing applications than the above traditional scintillators.

A drawback of  $\text{Rb}_2\text{LiYBr}_6:\text{Ce}^{3+}$  is the relatively low Li concentration. The absorption length of 0.18 nm neutrons in a 95%  ${}^6\text{Li}$ -enriched crystal is calculated to be  $\sim 3.5$  mm. This is smaller than 3.7 cm of total  $\gamma$ -ray attenuation length at 662 keV quanta. Compared to 0.54 mm of  ${}^6\text{LiI:Eu}^{2+}$ , the absorption length of 0.18 nm neutrons in  $\text{Rb}_2\text{LiYBr}_6:\text{Ce}^{3+}$  is large.<sup>8</sup> Therefore, relatively thick layers are needed for efficient neutron detection. However, the cubic elpasolite structure of this material allows the use of ceramic techniques to produce layers with good optical transmission. It should be noted that  $\text{Rb}_2\text{LiYBr}_6:\text{Ce}^{3+}$  is hygroscopic.

We gratefully acknowledge the support of Netherlands Technology Foundation (STW), the Swiss National Science Foundation, the European Community Research Infrastructure Action under the FP6 "Structuring the European Research Area" Programme (through the Integrated Infrastructure Initiative "Integrating Activity on Synchrotron and Free Electron Laser Science"), and Saint Gobain, division of crystals and detectors, Nemours, France.

<sup>1</sup>A. D. Taylor, *Physica B (Amsterdam)* **213–214**, 1037 (1995).

<sup>2</sup>K. Fox, *Nature* **438**, 730 (2005).

<sup>3</sup>D. Clery, *Science* **314**, 580 (2006).

<sup>4</sup>K. P. Nicholson and G. F. Snelling, *Br. J. Appl. Phys.* **6**, 104 (1954).

<sup>5</sup>L. R. Moras, *J. Inorg. Nucl. Chem.* **36**, 3876 (1974).

<sup>6</sup>A. Bessiere, P. Dorenbos, C. W. E. van Eijk, K. W. Krämer, and H. U. Güdel, *IEEE Trans. Nucl. Sci.* **51**, 2970 (2004).

<sup>7</sup>C. W. E. van Eijk, A. Bessiere, and P. Dorenbos, *Nucl. Instrum. Methods Phys. Res. A* **529**, 260 (2004).

<sup>8</sup>C. W. E. van Eijk, J. T. M. de Haas, P. Dorenbos, K. W. Krämer, and H. U. Güdel, *IEEE Trans. Nucl. Sci.* **NS12**, 239 (2005).

<sup>9</sup>M. D. Birowosuto, P. Dorenbos, C. W. E. van Eijk, K. W. Krämer, and H. U. Güdel, *J. Phys.: Condens. Matter* **18**, 6133 (2006).

<sup>10</sup>L. M. Bollinger and G. E. Thomas, *Rev. Sci. Instrum.* **32**, 1044 (1961).

<sup>11</sup>A. Syntfeld *et al.*, *IEEE Trans. Nucl. Sci.* **52**, 3151 (2005).